

Optical properties (0.1–25 eV) of Nb-Mo and other Nb-based alloys†

E. S. Black,* D. W. Lynch, and C. G. Olson

*Ames Laboratory—Energy Research and Development Administration
and Department of Physics, Iowa State University, Ames, Iowa 50011*

(Received 28 February 1977)

The dielectric functions of $\text{Nb}_x\text{Mo}_{1-x}$ alloys ($x = 0.2, 0.5, 0.8$) and of Nb with 10-at.% Zr, with 20-at.% V, and with 20-at.% Ta were determined in the 0.1–25 eV energy range. Some of the interband region below 3 eV can be interpreted on the basis of the rigid-band model for Nb-Mo while the large structure at 4–4.5 eV cannot be so interpreted in any of the alloys using existing bands. An examination of all the alloys shows that there probably are distortions of the bands due to strain and potential differences. The transitions beginning at about 9 eV, from the Fermi level to a flat band above, are seen to have delocalized final states. All the alloys show two volume and two surface plasmons like those of Nb and Mo.

I. INTRODUCTION

Niobium and molybdenum have nearly identical band structures, making their alloys appear to be describable by the rigid-band model. Such a model has been used by Pickett and Allen¹ to calculate the optical properties in the 1–5 eV region. In the following, we report our measurements of the 0.1–25 eV optical properties of several Nb-Mo alloys, as well as those of some alloys of Nb with its other neighbors in the periodic chart: V, Ta, and Zr. Both V and Ta are completely miscible in Nb, but their band structures are slightly different, as is the Fermi level with respect to band edges, despite identical valences. Here the rigid-band model is meaningless, for all effects are due to changes in the electronic structure. Zr itself is hcp rather than bcc and is soluble in Nb only up to about 10%.² A rigid-band model seems applicable to Nb-Zr alloys,³ but such a model requires the bands of hypothetical bcc Zr at the “proper” lattice parameter.

Our measurements cover not only the range of strong interband absorption involving states near the Fermi level, but also higher-energy regions in which electrons are excited from the Fermi level or below to states in non-free-electron-like bands 10 eV above the Fermi level. Moreover, we can compare our data with those of the pure metals measured previously^{4,5} both for interband absorption effects and plasmon phenomena. We conclude that the rigid-band model without electric-dipole matrix elements can explain the spectra for Nb-rich alloys with Mo in the 1–3 eV region, but it is poor at higher energies, that alloying does not cause major changes in optical selection rules, that two volume plasmons exist in all our alloys, as well as in the pure metals, that the higher-energy plasmon shifts as expected from a free-electron-gas model, and, finally, that there

is little additional damping of the plasmons in these alloys due to impurity scattering.

II. EXPERIMENTAL

Samples were spark-cut from electron-beam melted ingots. They were lapped on SiC, polished with Al_2O_3 down to 0.3- μm size, then heavily electropolished to remove spark-cutter and polishing damage, at least 50 μm being removed. They were then annealed and, just prior to optical measurements, given a light electropolish (6-vol % perchloric acid in methanol at dry-ice temperature).

The infrared, visible, and near ultraviolet measurements were made at 4 K by a calorimetric technique.⁶ The vacuum ultraviolet measurements were made at 300 K using synchrotron radiation from the electron storage ring, Tantalus I, at the Synchrotron Radiation Center of the University of Wisconsin. The techniques and apparatus have been described previously.⁷ The data processing, via Kramers-Kronig analysis, was identical to that used in our previous study of other bcc^{4,5} and hcp transition metals.⁸ The use of data taken at two different temperatures was not important, for in the region of overlap there was little temperature dependence,⁹ and the data taken by the two techniques and at two temperatures overlapped well. Alloy compositions, given in atomic percent, were determined by chemical analysis, and were virtually identical to the compositions expected from weighing the components before melting.

Errors in the data are only a few percent of the measured values. The extrapolations needed for the Kramers-Kronig analysis introduced larger errors in the dielectric function $\tilde{\epsilon} = \epsilon_1 + i\epsilon_2$ than did any measuring errors. A Drude reflectance was fitted to the data at low energy, the relaxation time

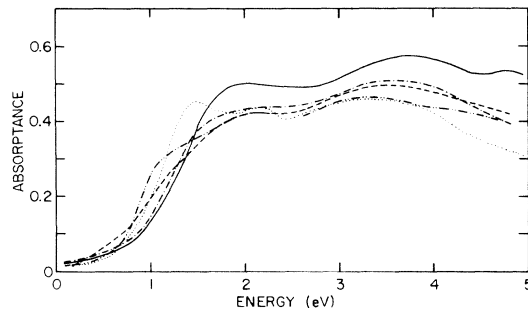


FIG. 1. Absorbance spectra of Nb (solid), Mo (dotted), and three Nb-Mo alloys at 4.2 K: dash-dot, 20-at. % Mo; dash, 50-at. % Mo; dash-double dot, 80-at. % Mo.

τ of which was found by fitting the measured absorbance at 0.1 eV to that expected for a free-electron gas (despite known interband absorption), $A = 2/\omega_p\tau$, with ω_p , the plasma frequency, determined from the composition, treating all d and conduction electrons as having an effective mass of unity. The neglect of interband absorption causes an erroneous low-energy extrapolation, which appears as an incorrect magnitude for the real and imaginary parts of the dielectric function. Peak positions and shapes, the features we will discuss, are given correctly for a number of reasonable infrared extrapolations. At higher energies, we had available the extrapolations used previously for the pure constituents of our alloys. (For V, we used other data¹⁰ believed to be taken on relatively oxide-free surfaces.) The extrapolations were chosen to conform to the measured absorption spectra of core electrons and to the sum rule on the absorption of such core electrons. For the alloys, we used composition-weighted averages of the extrapolations for the constituents. The errors in $\bar{\epsilon}$ due to high-energy extrapolation errors are also in the magnitudes, rather than the shapes, but when plasmons are discussed the characteristic-electron energy-loss function, $\text{Im}(-1/$

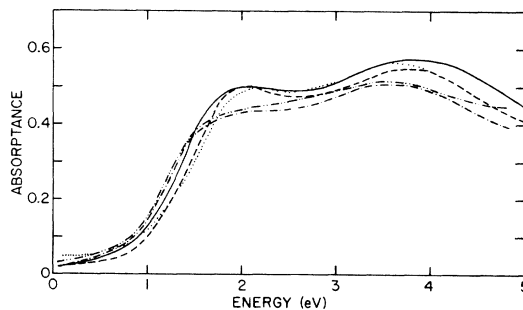


FIG. 2. Absorbance spectra of Nb (solid) and alloys of Nb with V, Zr, Mo, and Ta at 4.2 K: dash-double dot, 20-at. % V; dot, 10-at. % Zr; dash-dot, 20-at. % Mo; dash, 20-at. % Ta.

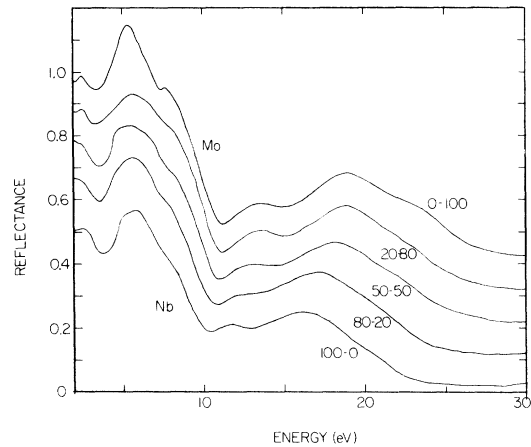


FIG. 3. Reflectance spectra of Nb, Mo, and three Nb-Mo alloys at 300 K. The ordinates are correct for Nb. The other curves have been shifted upward by 0.1 from the curve below.

$\bar{\epsilon}) = \epsilon_2/(\epsilon_1^2 + \epsilon_2^2)$, is needed. Peak heights and widths in this function are dependent on the magnitude of ϵ_2 . Moreover, the peak position occurs roughly at the energy at which ϵ_1 goes through zero, which is affected by the high-energy extrapolation. Since our previous calculated electron-energy-loss function spectra for Nb, Mo, and Ta were in good agreement with directly measured loss functions, and we used similar methods on similar data, we expect the peak positions not to be in error by any significant amount, but the heights and widths may not be meaningful.

Figures 1 and 2 show the absorbances of the alloys measured at 4 K. It is clear that no dramatic changes, either in structure appearance or disappearance, or in broadening occur. The positive slopes, dA/dE , at even the lowest energies indicate the presence of some interband absorption. Thus we do not display the Drude parameters which were used for the infrared extrapolation.

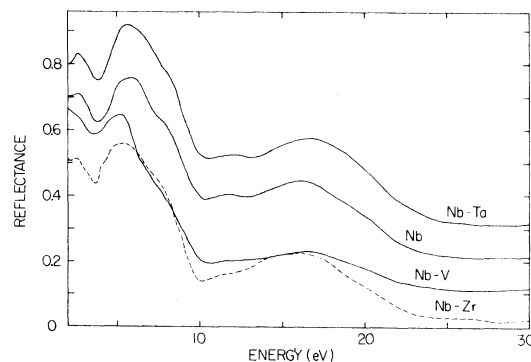


FIG. 4. Reflectance spectra of Nb and alloys of Nb with V, Zr, and Ta at 300 K. The ordinates are correct for Nb. The other curves have been shifted as on Fig. 3.

Their use to subtract free-electron effects at energies above 0.1 eV is questionable. Note also the sharp rise in A at about 1 eV. It does not broaden appreciably upon alloying, indicating no dramatic increase in scattering rates or a change in selection rules, e.g., from direct to indirect. The reflectances to 25 eV are shown in Figs. 3 and 4. Above about 5 eV, the reflectances of the Nb-Mo alloys are very close to these of composition-weighted averages of the reflectances of the two constituents. The Kramers-Kronig analysis of these data led to many spectra, too many to present. In the following, we present the spectra in whatever form proved most useful for interpretation in a particular spectral region.

III. RESULTS AND DISCUSSION

A. Interband absorption 1-10 eV

The gross features of the interband conductivities of these alloys are similar to those of Nb or Mo, already published.^{4,5,11} Figure 5 shows the conductivity of the Nb-Mo alloys. The intraband conductivity has not been subtracted out, for there is enough interband absorption at our lowest energy to preclude obtaining any meaningful Drude parameters. As can be seen in Fig. 5, the prominent peak at 5 eV in Nb shifts to lower energy and becomes somewhat larger as Mo is added. The 2.5-eV peak is unchanged, and a shoulder grows at 2 eV as Mo is added. (The region above 9 eV will be discussed later.) Figure 5 is similar to data recently published for the V-Cr,¹² Fe-Cr,¹³ and Ta-W-Re¹⁴ systems. The structure reported by Bol'shova and Leksina¹⁵ at 0.7 eV in the conductivity of Nb with 15-at. % Ti is not apparent in our conductivity spectrum for Nb with 10-at. % Zr.

Figure 6 shows the conductivity of the alloys of Nb with Zr, V, and Ta. The peak at 2.5 eV in Nb becomes a shoulder in all three alloys, while the addition of 20% Mo affects this peak very little. The peak at 5 eV in Nb is changed considerably by adding V or Ta, but in different ways, shifting considerably to lower energy and becoming weaker with V, and shifting to lower energy, but gaining strength with Ta.

Besides our initial interpretation^{3,4} of the structures in the optical conductivity of Nb and Mo, there are two more recent interpretations, based on band structures but using the full Brillouin zone, rather than just symmetry lines.^{1,16} Both interpretations were carried out for Mo, but unfortunately, they used different bands, different methods for assigning structure in the spectra, and obtained somewhat different interpretations. (Both assumed direct interband transitions and neglected

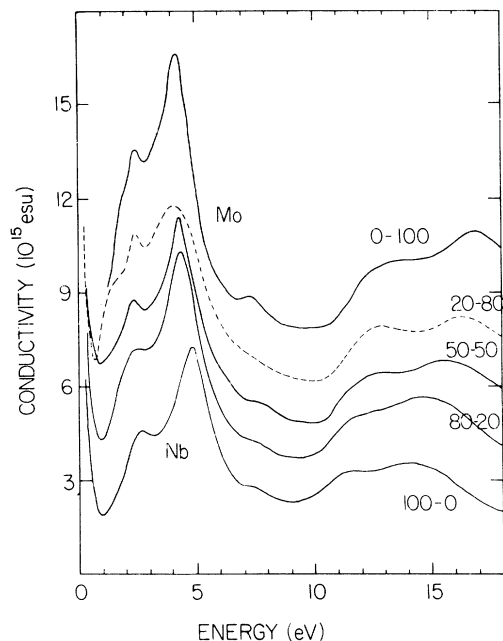


FIG. 5. Optical conductivity of Nb, Mo, and three Nb-Mo alloys obtained from a Kramers-Kronig analysis of the data in Figs. 1 and 3. The ordinates are correct for Nb. The other curves have been shifted upward 3 units from the curve below.

matrix elements, except those expected to be zero. One calculation showed that nondirect transitions could not be excluded by comparing experimental data with the calculation.¹⁶) One might hope that the different assignments for the interband structure could be distinguished by different predicted effects of the alloying of Nb with Mo. Table I shows this hope to be unfounded. The entries for the effect are based on the lowering of the Fermi level alone. A transition "weakens" if fewer initial

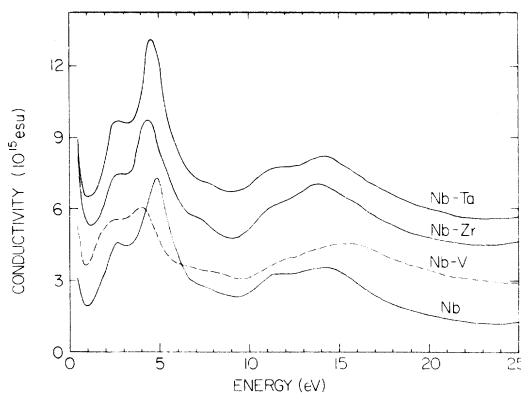


FIG. 6. Optical conductivity of Nb and alloys of Nb with V, Zr, and Ta obtained by Kramers-Kronig analysis of the data in Figs. 2 and 4. The ordinates are correct for Nb. The other curves have been shifted as in Fig. 5.

TABLE I. Identification of the origin of structure in the interband conductivity of Mo, and rigid-band-model prediction for the effect of Nb addition.

Structure	Position (eV)		Transition (Ref. 16)	Effect of Nb	Transition (Ref. 1)	Effect of Nb
	Expt.	Calc.				
Weak onset	~0.5
Strong onset	1.5	1.5	Δ, Σ, G	Σ shifts to higher E
Shoulder	1.8-1.9	2.2-2.3	Δ	vanishes	Γ, Σ	both vanish
Peak	2.4	2.4	Γ^a	vanishes	$\Sigma?$	weakens
	...	3-3.3	F, G, Σ	weakens
Shoulder	3.5
	...	4.0	Δ	weakens	$(2\pi/a)(\frac{1}{2} \frac{1}{4})$	none?
Peak	4.2
	...	4.42	D, N	none
	...	5	N	none	D	none
	...	5.6	F	none
	...	5.8	Λ	none
	...	6	Σ	none

^a Forbidden at the symmetry point or line.

states along (and near) a symmetry line remain below the Fermi level as the Fermi level drops. A transition "vanishes" if the lower Fermi level leaves all initial states on a line empty. A lower Fermi level could give rise to newly empty final states, but these do not seem to be important. In both cases, the designations of transitions with symbols for symmetry points and lines is used to denote volumes of k space near these points and lines. Actual critical-point structure is not expected to be prominent. Both sets of interpretations give about equal agreement with the curves of Fig. 5. The calculations¹ of the dielectric function of Nb and Mo give nearly the same structure at 4-4.5 eV, in agreement with the data on Nb, but in poor agreement for Mo, where the experimental peak is much larger. The calculation of Ref. 16 gives the 4-eV peak in Mo quite well, but does not consider Nb.

It should be pointed out that matrix elements are expected to be important. The transitions involved are derived from dipole-forbidden $d-d$ transitions on the atoms. These are allowed in the cubic crystal field, but they may vary from very weak to quite strong, partly depending on the amount of hybridization with the $s-p$ electrons. There has been only one limited attempt to study interband matrix elements in bcc transition metals,¹⁷ and a large k dependence was found. The transitions in Fig. 5 are not very forbidden. The sum rule on ϵ_2 shows that between 0.1 and 5 eV, 1.5 to 3 electrons per atom contribute.

To facilitate comparison with the rigid-band model and to exhibit differences between solutes ex-

pected from size or valence effects, we show in Figs. 7-9 the differences between the alloy conductivities and those of the pure metal nearest each in the periodic chart. (These curves still contain free-electron components of the conductivity, for our Drude parameters give values of conductivity that are too large above 1 eV because the interband absorption at low energies makes the relaxation time erroneously short.) These difference curves could be in substantial error because of errors in the magnitudes of the conductivities due to the extrapolations in the Kramers-Kronig integrals. However, both the reflectances and the extrapolations are all similar, and the errors in the magnitudes of the conductivities should be systematic, hence reduced in the difference plots. Moreover, the differences are large. These figures show error bars of 5% of the conductivity of Nb. From these, some of the small structures in the figures appear to be noise.

It is immediately evident from Fig. 7 that adding Mo and Zr to Nb have opposite effects on the conductivity edge at 1-1.5 eV, but similar effects on the peak at 5 eV and in the 10-20 eV region. For V and Ta, (Fig. 8) the effects are again opposite in the 1-1.5 eV region (V is like Zr; Ta is like Mo), but opposite in the 5-eV region as well. Ta produces little change above 10 eV, while V gives a change opposite to that caused by Mo and Zr. Figure 9 shows the effect of adding Mo to Nb and of adding Nb to Mo. Over most of the spectrum, one is nearly the negative of the other.

Figure 10 shows a comparison of our low-energy data with the rigid-band model calculations of

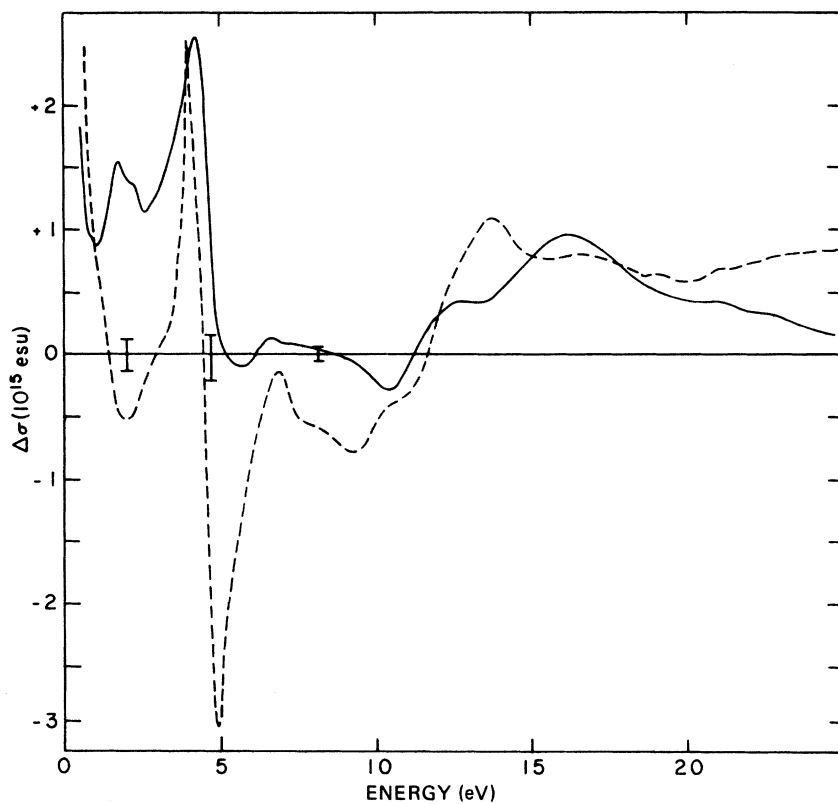


FIG. 7. Differences in optical conductivity. Solid line: $\text{Nb}_{0.8}\text{Mo}_{0.2}\text{-Nb}$. Dashed $\text{Nb}_{0.9}\text{Zr}_{0.1}\text{-Nb}$, but multiplied by 2 for normalization.

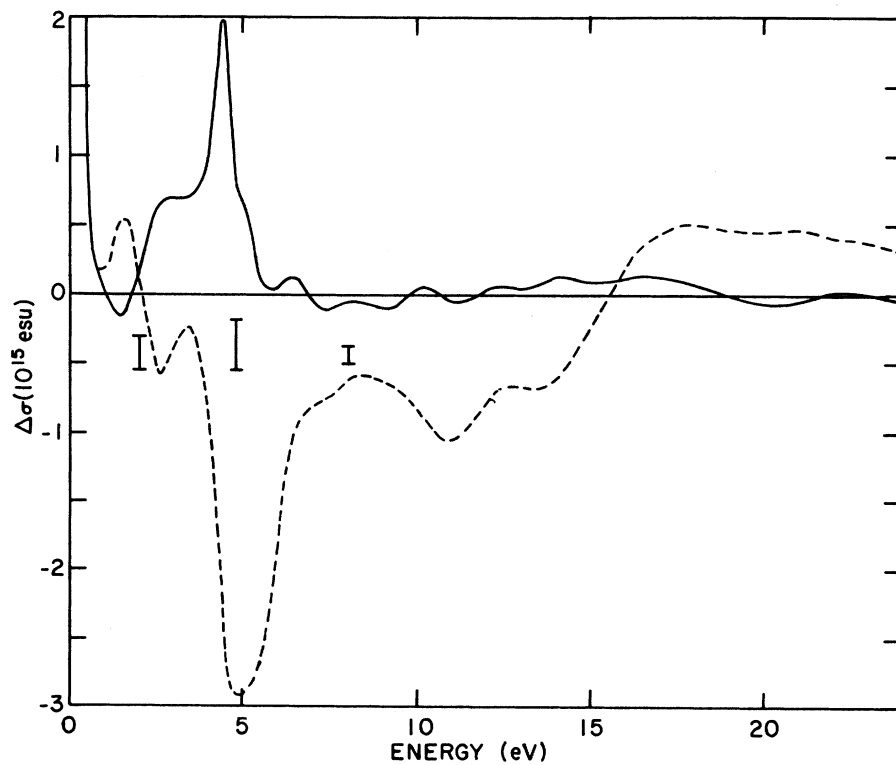


FIG. 8. Differences in optical conductivity. Solid: $\text{Nb}_{0.8}\text{Ta}_{0.2}\text{-Nb}$. Dashed line: $\text{Nb}_{0.8}\text{V}_{0.2}\text{-Nb}$.

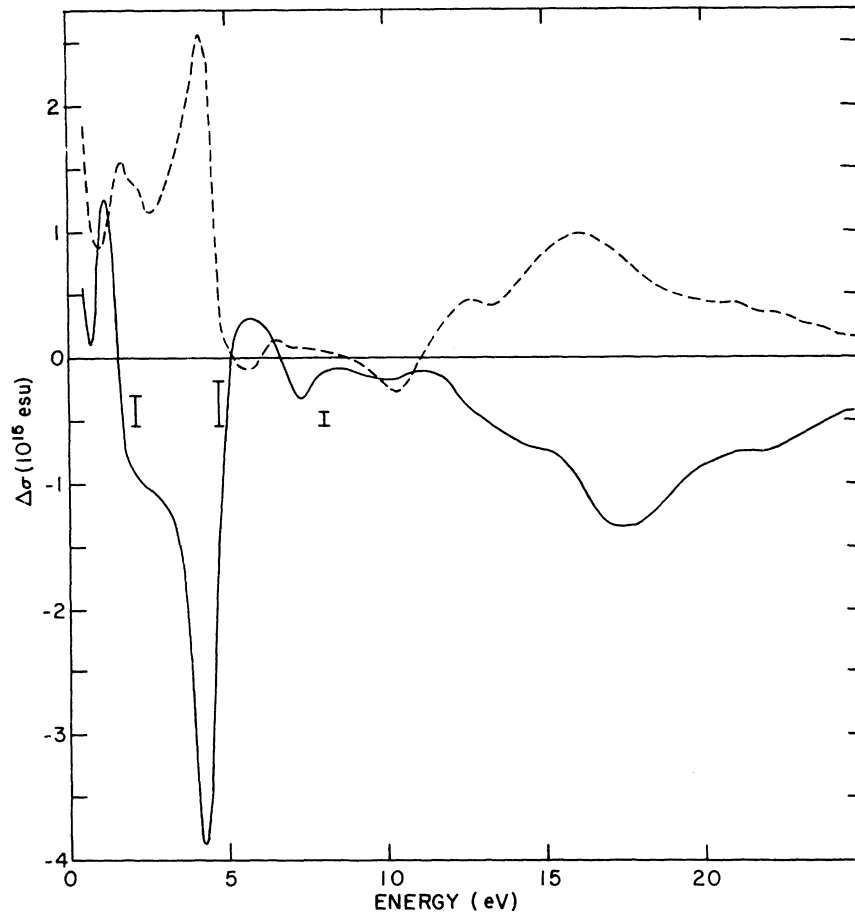


FIG. 9. Differences in optical conductivity. Solid line: $\text{Nb}_{0.2}\text{Mo}_{0.8}\text{-Mo}$. Dashed line: $\text{Nb}_{0.8}\text{Mo}_{0.2}\text{-Nb}$.

Pickett and Allen¹ for 20-at. % Mo in Nb and 20-at. % Nb in Mo. There is some quantitative agreement of the data with the calculated spectrum at the Nb-rich end of the system [Fig. 10(a)] but not at the Mo-rich end [Fig. 10(b)]. Above 2.5 eV there is little agreement with the calculations, for the

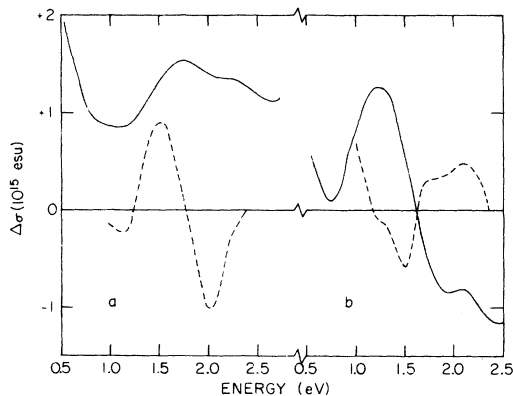


FIG. 10. Differences in optical conductivity as measured (solid) and calculated (dashed) in Ref. 1. (a) $\text{Nb}_{0.8}\text{Mo}_{0.2}\text{-Nb}$, (b) $\text{Nb}_{0.2}\text{Mo}_{0.8}\text{-Mo}$.

calculated difference spectra are very small, but the measured differences are fairly large. Adding Re to Mo does not give the shift of the 1.0–1.5 eV structure expected from the rigid-band model either.¹⁸ In the Mo-Nb case, however, the metal and alloy energy bands are assumed to be the *same*, only the Fermi level having shifted upon alloying. The structures in Fig. 10(b) can be explained in a simple way. The conductivity of the 20–80 alloy has a shoulder at about 1 eV (Fig. 5). There is a similar structure at about 1.4 eV in Mo (not shown in Fig. 5—see Ref. 5). This structure probably arises from $\Delta_5 \rightarrow \Delta'_2$ transitions, which split into Δ_6 , $\Delta_7 \rightarrow \Delta_7$ from the spin-orbit interaction. (This splitting has been resolved in thermomodulation measurements.⁹) As the Mo concentration drops from 100 to 50-at.%, the Fermi level drops below the region along Δ in which the bands are parallel, and this transition is lost. The shift of the shoulder to lower energy, expected because the bands under discussion become closer in energy at k_F as k_F drops when Nb is added to Mo, gives rise to the positive and negative peaks in the difference spectrum of Fig. 10(b). It is explained

qualitatively by the rigid-band model, but not accounted for in the work of Ref. 1. At the Nb-rich end, the expected positive peak appears in the spectrum, but there is no negative structure. The spectrum in this region does not arise from transitions along Δ , for the initial states are empty.

It is premature to say that the Nb-Mo spectra require a small change in the bands upon alloying. It is clear that a change easily could produce difference spectra as large as those found, for such is the case in the Nb-V and Nb-Ta systems. Here small and not-so-small changes in the energy bands are responsible for the entire difference spectra.

In order to interpret the data on the V and Ta alloys one must have, at the minimum, bands for both pure metals calculated by the same method. Mattheiss^{19,20} has calculated bands for Nb and Ta, while Alward *et al.*²¹ have done V and Ta. The techniques used for the calculations and the criteria for successful calculation were both different. This is evident when one notices that upon going from Nb to Ta Mattheiss finds the *d* bands broaden, but Alward *et al.* find *d*-band narrowing when going from V to Ta. One of the effects of adding V or Ta is a change in lattice parameter. Anderson *et al.*²² have calculated the bands for Nb at normal and reduced lattice parameter. Taking the fixed reference as the Fermi level, the bands recede from the Fermi level upon reduction of the lattice parameter, filled states dropping and empty states rising, which pushes all interband transitions to higher energy. (Dipole matrix element changes should occur as well.) Thus strain effects alone predict that all structures shift to lower energy upon adding Ta and to higher energy

upon adding V. Such shifts do indeed occur in the 1-1.5 eV region, but the shifts in the large 4-4.5 eV structure are in the wrong directions, although they are in opposite senses for the two solutes. In view of this state of affairs, and the fact that one should have more than a set of energy bands for the interpretation of optical spectra in metals, we postpone further interpretation of Figs. 7-9 for future theoretical study. (Recently, densities of states have been calculated for Nb-Mo alloys using the coherent potential approximation.²³ Below the Fermi level, the density of states of a 50-50 alloy resembles that of either metal, but there is additional structure in the alloy density of states above the Fermi level. It is not yet clear whether this can account for the observed changes in the conductivity. These calculations also indicate that there is very little disorder-induced scattering, as observed.)

B. Interband absorption 9-20 eV

The optical conductivity has a minimum around 9 eV (Figs. 5 and 6), then rises again. In previous work, we have attributed this rise to transitions from the Fermi level, and states just below, to a flat band about 10 eV above the Fermi level. This band has been seen in at least one calculation for a bcc transition metal,¹⁷ and there is evidence for it at lower energies in hcp transition metals and at higher energies in fcc transition and noble metals.

Looking first at the Nb-Mo series (Fig. 5) we see that the addition of increasing amounts of Mo to Nb moves the threshold for this absorption to higher energy by about 1.8 eV. The shift is roughly linear with Mo concentration. The shoulder at 11 eV in Nb similarly shifts upon Mo addition, about 2.5 eV for 100% Mo, and it grows in strength. The peak shifts a total of about 2.5 eV; also it shifts about linearly with composition, and it, too, grows. This shift is in the wrong direction for the simplest rigid-band model, for as Mo is added to Nb, the Fermi level rises, making a red shift expected. This unexpected shift can, however, be allowed by the rigid-band model. Each set of bands is expected to shift rigidly by some average of the perturbing potential, but all bands need not have the same average shift, especially if there is considerable difference in radial distribution of the charge densities around the atoms for different bands.

That these edges shift is significant, for it implies that the final state is not localized on one site. If there were such localization, the alloy spectra in this region should resemble a weighted average of the spectra of the components, and the

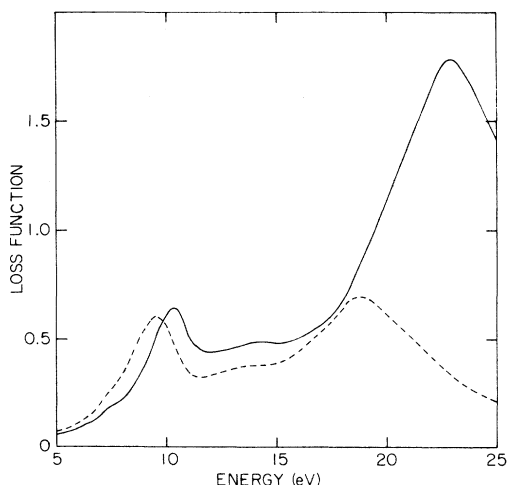


FIG. 11. Characteristic electron-energy-loss functions for $\text{Nb}_{0.5}\text{Mo}_{0.5}$. Solid: volume loss function, $\text{Im}[-1/\epsilon]$. Dashed: surface loss function, $\text{Im}[-1/(\epsilon+1)]$.

TABLE II. Peak positions (eV) of electron-energy-loss functions.

Sample	$\text{Im}(-1/\bar{\epsilon})$	Peaks	$\text{Im}[-1/(\bar{\epsilon}+1)]$	Peaks
Nb	9.8	20.85	9.0	17.2
Nb ₈₀ Mo ₂₀	10.1	21.8	9.4	18.2
Nb ₅₀ Mo ₅₀	10.35	23.0	9.6	18.7
Nb ₂₀ Mo ₈₀	10.5	23.65	9.6	19.2
Mo	10.5	24.6	9.6	20.0
Nb ₈₀ V ₂₀	9.5	20.6	8.4	17.4
Nb ₈₀ Ta ₂₀	9.8	21.0	9.2	17.5
Nb ₉₀ Zr ₁₀	9.4	20.8	9.8	18.3

edge at 9.0 eV in Nb would weaken, but not shift as Mo is added. Such a superposition was reported by Beaglehole and Thiéblemont²⁴ for Cu-Au alloys. It would be useful to extend band calculations for bcc metals to higher energies, as Christensen²⁵ has done for Au, to see if the flat band shifts in the "proper" direction (upwards) with increasing atomic number.

Plots of the characteristic electron-energy-loss function, of which Fig. 11 is typical, show that in each of these alloys, as in many bcc transition metals, there are two longitudinal collective excitations, one near the free-electron plasmon energy and one much lower, lying in the region of the minimum in ϵ_2 . There are, similarly, two peaks in the loss function for surface excitations, indicative of two surface plasmons. All loss-function peak positions are given in Table II. Figure 11 shows that for the 50-50 alloy, as for all the others measured, there is little or no extra damping of these plasmons introduced by the alloying, insofar as there are no systematic effects of alloying on the peak heights and widths of the peaks. (There will be errors in the peak heights due to inaccuracies in the absolute values of the dielectric-function components as a result of the Kramers-Kronig analysis.)

As has been noted, the higher-energy plasmon in bcc and hcp transition metals (and in fcc transition metals as well) is usually very close to the free-electron value, $\omega_p = (4\pi Ne^2/m)^{1/2}$. In Fig. 12 we have plotted the

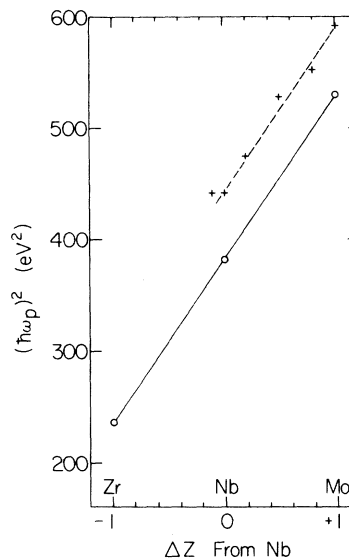


FIG. 12. Square of the plasma frequency vs composition. See text.

square of the energy of the higher energy observed peak in the loss function as a function of the electron concentration, assuming for the alloys that the volume changes are small enough that Vegard's law can be used. The line shows the strict free-electron-gas behavior, while the points show the actual data. There is a displacement of the data from the line, an effect of interband transitions, but the slope is remarkably parallel to that of the free-electron model. By extrapolating the bcc Nb-Mo line backwards, we get the region of the hypothetical bcc Nb-Zr, including bcc Zr. The observed hcp Zr plasmon falls right on the extrapolation for bcc Zr.

ACKNOWLEDGMENTS

The alloys were produced by F. A. Schmidt of the Ames Laboratory. The Synchrotron Radiation Center is supported under NSF Grant No. DMR-7415089. We wish to thank E. S. Giuliano for interesting correspondence, and J. H. Weaver for helpful discussions.

†Work performed for the U. S. ERDA under Contract No. W-7405-eng-82.

*Present address: Rocketdyne Division of Rockwell International, Canoga Park, Calif. 91304.

¹W. E. Pickett and P. B. Allen, Phys. Rev. B **11**, 3599 (1975).

²M. Hansen, *Constitution of Binary Alloys* (McGraw-Hill, New York, 1958).

³B. N. Harmon (private communication).

⁴J. H. Weaver, D. W. Lynch, and C. G. Olson, Phys. Rev. B **7**, 4311 (1973).

⁵J. H. Weaver, D. W. Lynch, and C. G. Olson, Phys. Rev. B **10**, 501 (1974).

⁶L. W. Bos and D. W. Lynch, Phys. Rev. B **2**, 4567 (1970).

⁷C. G. Olson and D. W. Lynch, Phys. Rev. B **9**, 3159

- (1974).
- ⁸D. W. Lynch, C. G. Olson, and J. H. Weaver, *Phys. Rev. B* 11, 3617 (1975).
- ⁹J. H. Weaver, C. G. Olson, D. W. Lynch, and M. Piacentini, *Solid State Commun.* 16, 163 (1975); J. H. Weaver, D. W. Lynch, C. H. Culp, and R. Rosei, *Phys. Rev. B* 14, 459 (1976).
- ¹⁰A. Seignac and S. Robin, *C. R. Acad. Sci. B* 271, 919 (1970).
- ¹¹B. W. Veal and A. P. Paulikas, *Phys. Rev. B* 10, 1280 (1974).
- ¹²M. M. Kirillova and L. V. Nomerovannaya, *Opt. Spektrosk.* 39, 540 (1975) [*Opt. Spectrosc.* 39, 303 (1975)].
- ¹³N. Ya. Gorban, V. S. Stashchuk, and M. F. Chernomorets, *Opt. Spektrosk.* 38, (1975) [*Opt. Spectros.* 38, 568 (1975)].
- ¹⁴L. K. Thomas and S. Thurm, *J. Phys. F* 6, 279 (1976).
- ¹⁵K. V. Bol'shova and I. Ye. Leksina, *Phys. Metal. Metalloved.* 29, 777 (1970) [*Phys. Met. Metallogr.* 29, No. 4, 101 (1970)].
- ¹⁶D. D. Koelling, F. M. Mueller, and B. W. Veal, *Phys. Rev. B* 10, 1290 (1974).
- ¹⁷I. Petroff and C. R. Viswanathan, *Phys. Rev. B* 4, 799 (1971).
- ¹⁸S. K. Behl and H. D. Drew, *Phys. Status Solidi B* 74, 721 (1976).
- ¹⁹L. F. Mattheiss, *Phys. Rev. B* 1, 373 (1970).
- ²⁰L. F. Mattheiss, *Phys. Rev. B* 1, 373 (1970).
- ²¹J. F. Alward, C. M. Perlov, C. Y. Fong, and C. G. Sridhar (unpublished).
- ²²J. R. Anderson, D. A. Papanconstantopoulos, J. W. McCaffrey, and J. E. Schirber, *Phys. Rev. B* 7, 5115 (1973).
- ²³E. S. Giuliano (private communication).
- ²⁴B. Beaglehole and B. Thiéblemont, *Nuovo Cimento* (to be published).
- ²⁵N. E. Christensen, *Phys. Rev. B* 13, 2698 (1976).